Arabian Journal of Chemistry (2018) 11, 871–879

King Saud University

Arabian Journal of Chemistry

www.ksu.edu.sa
www.sciencedirect.com

# Synthesis of highly water-dispersible N-doped anatase titania based on low temperature solvent-thermal method

**Wenyi Huang [1], Hao Cheng [1], Jun Feng, Zhipeng Shi, Dawei Bai, Lijun Li ***

*Guangxi Key Laboratory of Green Processing of Sugar Resources, College of Biological and Chemical Engineering, Guangxi University of Science and Technology, Liuzhou 545006, China*

Received 30 August 2017; accepted 21 December 2017
Available online 28 December 2017

**KEYWORDS**

$TiO_2$ nanoparticle;
Highly aqueous dispersion;
Visible light photocatalytic activity

**Abstract** In this paper, the high-concentration aqueous dispersion N-doped anatase $TiO_2$ is prepared based on low temperature non-aqueous solvent-thermal method by using $TCl_4$ and $NH_4Cl$ as titanium source and nitrogen source respectively. From TEM image, we can learn that the particle is composed of spindle-shaped particles with the size from 8 to 15 nm. According to the XRD and XPS spectra of N-doped $TiO_2$, it can be seen that, during the synthesis process, N atoms permeate into the $TiO_2$ lattice, and the impurity level can be formed within the band gap of $TiO_2$. The impurity level can extend to absorb UV and the visible light. As for N-doped $TiO_2$ nanoparticle of XPS spectrum, ethanol is used as solvent to form carbonaceous species on the surface of $TiO_2$. The carbonaceous species in visible light can excite electrons towards the $TiO_2$ conduction band, so as to increase the number of electrons in the conduction band under visible light to improve the catalytic activity of $TiO_2$ which possesses the feature of high catalytic activity under UV–visible light.


## 1. Introduction

Semiconductor-based photocatalysts are a class of advanced materials because of important applications to cleaning environmental pollution and producing new energy, such as degradation of organic pollutants and $H_2$ evolution from water-splitting under UV or visible-light irradiation. Due to its non-toxic and inexpensive, Titanium dioxide ($TiO_2$), as a semiconductor-based photocatalysts, has aroused extensive attention ( Kumar et al., 2012; Katoh et al., 2010; Dette et al., 2014; Periyat et al., 2009; Sun et al., 2012; Sukor et al., 2017; Hassan et al., 2017). $TiO_2$ has a wide band gap with 3.0–3.2 eV, which makes it has strong absorption capacity in the UV range and little absorption capacity in the visible range. This property restricts catalytic activity in the visible light range. At the same time, in order to obtain excellent photocatalysis properties, $TiO_2$ materials are usually made into products with nano scale. $TiO_2$ nanoparticles have high speci-

* Corresponding author.
E-mail address: lilijun0562@sina.com (L. Li).
[1] These authors contributed equally to this work and should be considered co-first authors.

Peer review under responsibility of King Saud University.

ELSEVIER Production and hosting by Elsevier

https://doi.org/10.1016/j.arabjc.2017.12.028
1878-5352 

fic surface area and own strong surface energy, which makes it agglomerate in water easily and arouse photocatalysis activity to decrease greatly. These aforementioned shortcomings have often prevented $TiO_2$ materials from further being applied to different fields.

To enhance the catalytic activity of $TiO_2$ under visible light, doping of $TiO_2$ with different elements, including wildly being explored both metallic and nonmetallic elements. Doping will help bring impurity level in the band gap, and then the impurity level can create splitting of energy levels of $TiO_2$. In this way, absorption under visible light can be improved. At the same time, doping also helps form crystal defects, which can reduce the rate of electron-hole recombination, thereby improving the efficiency of photocatalytic reaction. Kubacka's group prepared N,W-codoped $TiO_2$ using ammonium tungsten oxide as nitrogen source and tungsten source, Triton X-100 as surfactant and hexanol as cosurfactant, and then maintaining calcine under 500 °C. The N,W-codoped $TiO_2$ has high photocatalytic activity, but it can't disperse in water (Periyat et al., 2009; Halim et al., 2017; Rahman et al., 2017). Elaine's group uses tungstic acid and melamine borate as dopants to prepare C, W co-doped $TiO_2$ under the 400 °C calcination, and the result shows that W atoms can diffuse into the $TiO_2$ lattice, which instead increases in visible-light activity of $TiO_2$. However, high-temperature calcination would lead $TiO_2$ to agglomerate. The agglomeration of $TiO_2$ greatly decreases the dispersion in aqueous solution (Elaine et al., 2012; Basheer et al., 2017; Ismail and Hanafiah, 2017). Di Li's group had used high-temperature treatment device for atomizing to prepare F,N-codoped $TiO_2$ (Li et al., 2005; Aziz and Hanafiah, 2017) . This F,N-codoped $TiO_2$ has some capacity for absorbing visible light, but the dispersibility in water is poor. Sakthivel's group synthesized N doped $TiO_2$ using thiourea as N source. The band gap of obtained $TiO_2$ can decrease to 2.91 eV, but it would agglomerate after calcination at 400–600 °C. In this way, the dispersibility becomes worse (Sakthivel et al., 2004; Khan et al., 2017). Doping can more or less improve the photocatalysis activity of $TiO_2$ under visible light. However, high temperature calcination in these methods often lead the obtained $TiO_2$ can hardly disperse in water (Elaine et al., 2012; Jobbagy et al., 2008; Kiraz et al., 2011; Sakthivel et al., 2004; Tachikawa et al., 2004; Chen et al., 2007; Serpone, 2006; Li et al., 2005; Shamsudin et al., 2017; Ghafar et al., 2017).

To improve the dispersible property of $TiO_2$ nanomaterials in water, surface modification with organic chelating ligands, such as oleic acid, oleate, and dopamine is a common method. Surface modification can reduce the number of surface hydroxyl groups, thereby reducing the $TiO_2$ surface energy and increasing the dispersibility of $TiO_2$. For instance, tetrabutylammonium modified $TiO_2$ nanoparticles dispersed both in the water and ethanol, but tetramethylammonium modified $TiO_2$ nanoparticles can only disperse in water (Chen et al., 2007; Razali and Said, 2017). Surface modification of dopamine is responsible for controlling the morphology, crystallinity, phase selection, and water dispersion of $TiO_2$ (Tahir et al., 2006; Halim and Phang, 2017). However, the $TiO_2$ catalytic reaction is mainly carried out in the particles surface. Surface modification may increase the thickness of the $TiO_2$ surface and reduce the activity of $TiO_2$ response to light. Efficiency of the catalytic reduction of $TiO_2$, therefore, is lower. Thus, how to greatly improve $TiO_2$ dispersion without surfactant modification is a challenging and meaningful task (Ai et al., 2014).

For study, we choose $NH_4Cl$ as the nitrogen source to synthesize N-doped $TiO_2$ nanoparticle. Since the radius of an oxygen atom and a nitrogen atom are similiar, in the preparation process, the nitrogen atoms can directly dop into the $TiO_2$ lattice without calcination process. Meanwhile, by avoiding the heat treatment and surface modification, the obtained $TiO_2$ not only can disperse easily in water, but also has significant catalytic activity under visible light. Most importantly, this method is simple with no strict requirements for equipment. It can easily achieve large-scale industrial production with high dispersion and significant catalytic activity by this method.

## 2. Experimental section

### 2.1. Synthesis of $TiO_2$ nanoparticles

Firstly, 0.3 g $NH_4Cl$ is added to 50 ml of ethanol, stirring at 60 °C for 30 min. After 30 min, part of $NH_4Cl$ solid has been dissolved and the mixture solution, filtrated by filter paper to obtain saturated $NH_4Cl$ solution. Then, 30 ml $TiCl_4$ is pumped into the saturated $NH_4Cl$ solution carefully by peristaltic pump under constantly stirring at room temperature, and the solution would change from colorless to yellow color. After $TiCl_4$ is pumped, the yellow solution is stirred for another 5 min, then moved into reaction kettle (Teflon), and heated at 150 °C for 5 h. Next, the reaction kettle is cooled at room temperature and a white solid is obtained. The solid is washed three times with 50 ml of ethanol each time, and subsequently dried at 55 °C for 45 min. The resulting product is powdered for further experiment and characterizing. Without adding $NH_4Cl$, the undoped $TiO_2$ nanoparticles can be prepared in the same method.

### 2.2. Characterization

The crystal phases of $TiO_2$ nanoparticles were identified in accordance with X-ray diffraction (XRD) patterns on a Bruker D8 Advance X-ray diffractometer with Cu Ka radiation. The morphology of $TiO_2$ nanoparticles was observed by high-resolution transmission electron microscopy (HRTEM) on a JEOL JEM-2010 electron microscope at 200 kV. The TEM samples were prepared by dispersed $TiO_2$ nanoparticles powder in water and then dropped on carbon–copper grid. Finally, the copper grid deposited with $TiO_2$ nanoparticles were observed by HRTEM. X-ray photoelectron spectroscopy (XPS) was recorded with a Kratos ASIS-HS X-ray photoelectron spectroscope equipped with a standard and monochromatic source (AlKR) at 150 W (15 kV, 10 mA). The binding energies obtained in the XPS analysis were corrected for specimen charging by referencing the C 1s line to 284.5 eV. The optical absorption spectra of the samples were recorded by UV–vis spectra at room temperature with the UV–visible spec-trophotometer equipped with an integrated sphere. Thermal gravimetry analysis was determined on STA 409 PC Luxx differential scanning calorimetry-thermo-gravimetric (DSC-TG) at the heating rate of 10 °C $min^{-1}$ under nitrogen condition.

*2.3. Study on photocatalytic properties*

For the photocatalytic property of prepared $TiO_2$ nanoparticle, solar light and LED lamp are used as light source to degrade methylene blue. Firstly, $6.7 \times 10^{-5}$ M methylene blue solution was prepared by dissolving 0.01 g methylene blue in 400 ml deionized water. Next, 0.25 g prepared $TiO_2$ nanoparticle powder was added to 50 ml of methylene solution with blue color and the powder and solution were mixed uniformly. According to the method, the desired concentration (0.5 g/L) of $TiO_2$-methylene blue solution can be obtained. Finally, to study the photocatalytic activity of prepared $TiO_2$ nanoparticle, $TiO_2$-methylene blue solution was divided into two parts and placed under the sunlight and LED light respectively. To monitor the reaction process for photocatalytic degradation, the UV–vis spectra of $TiO_2$-methylene blue solution was measured in the same time interval during the photocatalytic activity experiments.

## 3. Results and discussion

*3.1. Characterizations of $TiO_2$ nanocrystals*

Fig. 1 refers to the TEM image of N-doped $TiO_2$ nanoparticle in different amplifications. TEM image analysis reveals that the as-prepared N-doped $TiO_2$ nanoparticle is spindle-shaped particles with the size from 8 nm- to 15 nm. Fig. 1(c) further displays the higher magnification of the nanocrystal lattice fringes of (1 0 1) crystallographic planes with lattice space of 0.36 nm in Fig. 1(d).

Fig. 2 shows the XRD spectra of N-doped $TiO_2$ drying at different temperatures. The peaks with the position of 25.3, 37.68, 47.82, 53.74, 55.16, and 62.57, are represented to (1 0 1), (0 0 4), (2 0 0), (1 0 5), (2 1 1), (2 0 4) planes, respectively. The XRD result proves that as-prepared N-doped $TiO_2$ nanoparticles dried in different temperature are all anatases (Ai et al., 2014; Yurdakal et al., 2008; Du et al., 2013). Based on Scherrer formula, it can be calculated that the average particle size of the prepared $TiO_2$ are 8.72 nm, 9.00 nm and 12.33 nm at 45 °C, 55 °C and 65 °C respectively, and the calculated diameter is similar to that of electron microscopy. It can be easily concluded that the average particle size of $TiO_2$ nanoparticles gradually increases with the drying temperature increasing also. Meanwhile, the intensity peaks of XRD also increases with the drying temperature rising. Hence, the degree of crystallinity of $TiO_2$ also increases with the drying temperature increasing. The peak intensity of $TiO_2$ nanoparticles drying under 45 °C is lower than that of the standard anatase $TiO_2$, that is, the degree of crystallinity of $TiO_2$ drying under 45 °C is insufficient. When the temperature is 55 °C and 65 °C, the intensity of peak is higher than that of standard anatase $TiO_2$. From 55 °C to 65 °C, the increasing scale of the peak intensity is not obvious. It indicates that the degree of crystallinity $TiO_2$ nanoparticles reaches a maximum drying degree under 55 °C.

Fig. 3a shows the XPS spectra of N-doped $TiO_2$ nanoparticle. In this spectrum, it can be found easily that the peaks of O1s, Ti2p, N1s, C1s, and Cl2p. in Fig. 3b is the XPS spectra of Ti2p. From the figure, the peaks at 458.98 eV and 464.68 eV represent $Ti2p_{3/2}$ and $Ti2p_{1/2}$, respectively (Yu et al., 2009; Zhang et al., 2015; Asahi et al., 2014; Zhu et al., 2009).

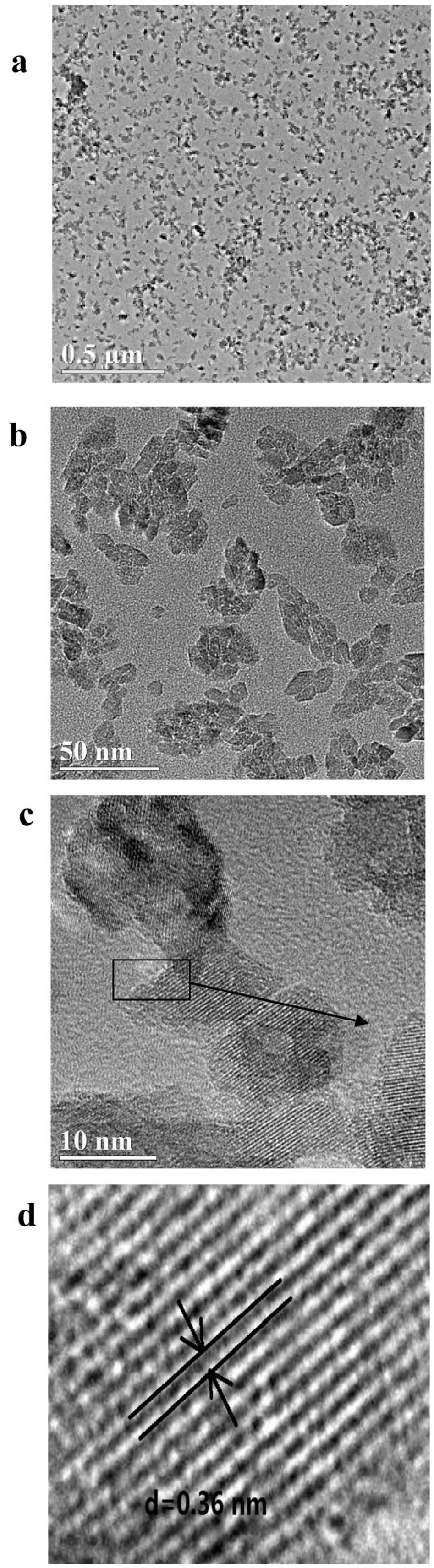


**Fig. 1** TEM of $TiO_2$ drying at 55 °C.

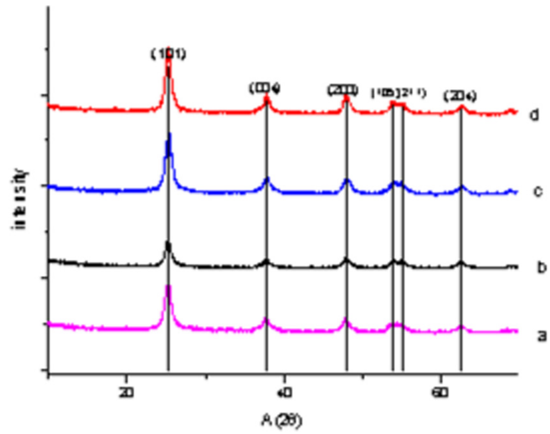


**Fig. 2** XRD spectra of N-dioped $TiO_2$ dried at different temperatures. (a) Standard anatase $TiO_2$, (b) N-dioped $TiO_2$ dried under 45 °C, (c) N-dioped $TiO_2$ dried under 55 °C, and (d) N-dioped $TiO_2$ dried under 65 °C.

Fig. 3c shows the XPS spectra of N1s. The XPS spectra of N1s can be fitted by two peaks centered at 399.78 eV and 400.25 eV respectively. The peak of 400.25 eV can be ascribed to Ti—N—O linkage. And the peak of 399.78 eV mainly comes from the $NH_4Cl$ which is adsorbed on the surface of $TiO_2$ nanoparticle (Li et al., 2005; Asahi et al., 2001; Irie et al., 2003; Kumar et al., 2013; Cong et al., 2006; Yu et al., 2009; Zhu et al., 2009). Comparing the intensity of two peaks, it can be inferred that the doped nitrogen atoms of $TiO_2$ nanoparticle mainly come from the nitrogen atoms which enter the crystal lattice of the $TiO_2$ nanoparticle to form Ti—N—O linkage, and a small of nitrogen atoms from the $NH_4Cl$ which is absorbed on the surface of $TiO_2$ nanoparticle. Fig. 3d refers to the XPS spectra of C2s, the three peaks of C2s at 284.66 eV, 286.11 eV and 288.78 eV, respectively. The peak at 284.66 eV is attributed to pure carbon (C—C). It results from the adsorbed carbon on the surface of the sample during the XPS sample pretreatment. Also, the other two peaks can be ascribed to carbon bound to oxygen (C—O) (Huang et al., 2008). It is indicated that carbon atom can be introduced into the system when ethanol is used as the solvent for preparation of N-doped $TiO_2$ nanoparticle.

XPS data shows that $NH_4Cl$ is used as the nitrogen source, ethanol as the solvent, except for a part of nitrogen doped into the space lattice of titanium dioxide. At the same time, epibiotic ammonium chloride and carbon can be adsorbed onto the surface of $TiO_2$. The O replaced by N will form defects, which facilitate to introduce impurity level to the forbidden band. Introducing impurity level helps decrease the recombination of electric-hole pairs and increase the utilization rate of light.

Fig. 4 is the TG of N-doped $TiO_2$ nanoparticle. As shown in step1, when the temperature increases from 30 °C to 161.8 °C under $N_2$ flow, the weight loss of N-doped $TiO_2$ is 0.8 mg, and the weight loss rate, 7.06%. It can be the water absorbed on the surface of $TiO_2$ nanoparticle, and the boiling point of water is 100 °C. Therefore, the weight losses in step 1 probably mainly come from the water evaporation. From 161.8 °C to 700 °C, the loss rate begins to decrease and quality

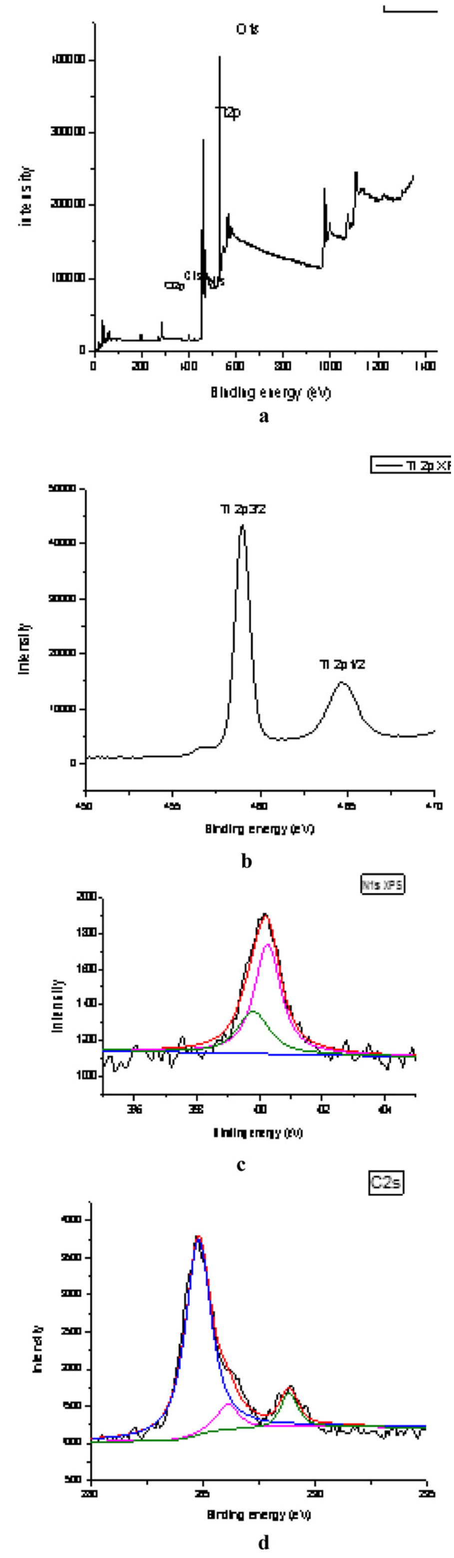


**Fig. 3** XPS spectra of $TiO_2$ nanoparticle. (a) the full XRD spectrum of $TiO_2$ nanoparticle, (b) XRD spectra of Ti2p, (c) XRD spectra of N1s, and (d) XRD spectra of C2s.

stabilizes to approximating 700 °C. In this step, the mass loss is 0.68 mg. It is speculated that the weight loss results from carbonizing carbon components on the surface of $TiO_2$.

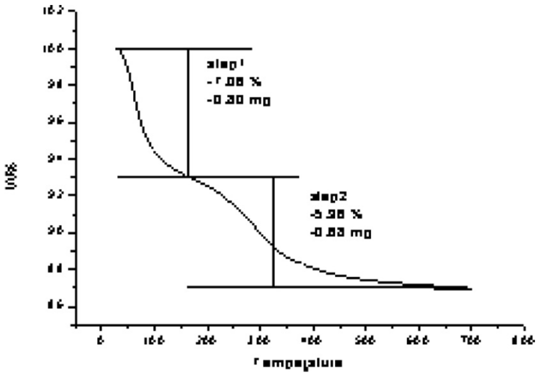

**Fig. 4** The TG of N-doped $TiO_2$ nanoparticle.

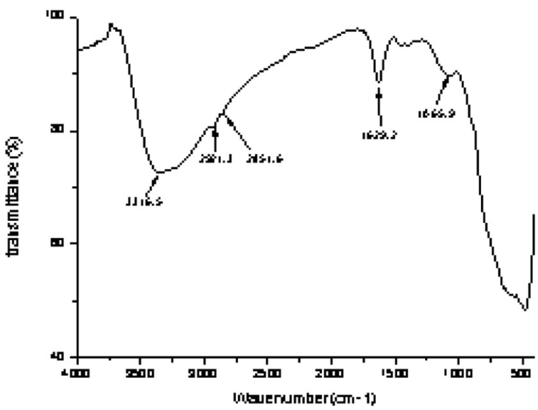


**Fig. 5** FT-IR spectrum of N-doped $TiO_2$ nanoparticle.

Fig. 5 is the FT-IR spectrum of N-doped $TiO_2$ nanoparticle. Above 2000 $cm^{-1}$, the FT-IR spectrum is dominated by the broad bands of O—H and N—H centered at 3300 $cm^{-1}$, which is greatly determined by C—OH groups or N—OH groups. The C—H stretching vibrations of the —$CH_2$— groups of the hydrocarbon at 2921.3 $cm^{-1}$ and 2851.6 $cm^{-1}$ are observed. The peak at 1629.2 $cm^{-1}$ comes from N—H bending vibration, and the peak at 1065.9 $cm^{-1}$ is attributable to C—N stretching vibration (Tian et al., 2011; Shan and Demopoulos, 2010; Han et al., 2012). FT-IR spectrum confirms that carbonaceous species and nitrogenous species exist, including C—H, C—O, C—N, N—H, and N—O. From the aforementioned XPS, TG and FT-IR characterizations, the saturated $NH_4Cl$ ethanol solutions can introduce carbonaceous species and nitrogenous species. By introducing carbonaceous species and nitrogenous species, the surface defect states of $TiO_2$ can be changed and agglomeration can be prevented. Also, it helps endow with the property of highly water dispersiblility and photocatalytic properties.

Fig. 6 shows the UV–vis spectrum of undoped $TiO_2$ nanoparticle and N-doped $TiO_2$ nanoparticle in different concentrations of $NH_4Cl$. With the increasing amount of $NH_4Cl$ in ethyl alcohol, in the visible region, the absorbance rate of $TiO_2$ gradually increases. In the ultraviolet region from 350 to 400 nm, the change is significant. However, regularity remained unchanged. From 400 to 600 nm, with the increase in the amount of $NH_4Cl$ in ethyl alcohol, the absorbance of N-doped $TiO_2$ nanoparticle gradually helps increase regularity. The result shows that under visible light, doping N atoms into $TiO_2$ can improve the absorbance of $TiO_2$. Fig. 7 shows the curve of energy gap calculated based on Kubelka-Munk function $[F(R\infty)E]^2$ vs the energy of absorbed light. From the extension cord of the curve, the energy band gap can be calculated as 3.33 eV, 3.30 eV, 3.21 eV and 3.15 eV for undoped $TiO_2$, 0.6 g/L $NH_4Cl$ N-doped $TiO_2$, 3.0 g/L $NH_4Cl$ N-doped $TiO_2$, and 6.0 g/L $NH_4Cl$ N-doped $TiO_2$ respectively . It is obvious that with the increasing amount of N atoms in $TiO_2$ nanoparticle, the band gap of $TiO_2$ nanoparticle becomes smaller.

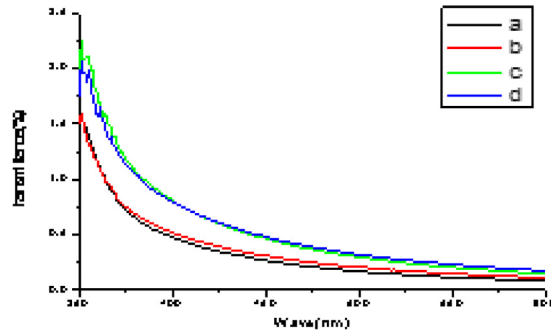


**Fig. 6** UV–vis spectrum of N-doped $TiO_2$ nanoparticle prepared in different concentration of $NH_4Cl$. (a) Undoped $TiO_2$ nanoparticle, (b) N-doped $TiO_2$ nanoparticle prepared in 0.6 g/L $NH_4Cl$ EtOH solution, (c) N-doped $TiO_2$ nanoparticle prepared in 3.0 g/L $NH_4Cl$ EtOH solution, and (d) N-doped $TiO_2$ nanoparticle prepared in 6.0 g/L $NH_4Cl$ EtOH solution.

### *3.2. Photocatalytic degradation of methylene blue with highly water dispersible N-TiO2 nanoparticle*

In order to assess the photocatalytic activity of water-dispersible N-doped $TiO_2$ nanoparticle under visible light, LED was used as the visible light source to degrade methylene blue. Figs. 8 and 9 are the UV–vis spectrum of methylene blue solution after degraded by different $TiO_2$ nanoparticles. With the comparison with the absorbance at 650 nm, it can be found that N-doped $TiO_2$ nanoparticle can completely degrade methylene blue by irradiating 5 h under LED light. However, commercially available undoped $TiO_2$ nanoparticle cannot be degraded completely. This suggests that as-preparation N-doped $TiO_2$ nanoparticle has high light response to visible light, and it can further prove that N-doped $TiO_2$ nanoparticle has a smaller energy level comparing with undoped $TiO_2$ nanoparticle.

As Fig. 10a shows, it is clear that the degradation rate of methylene blue by N-doped $TiO_2$ nanoparticle is faster than that of commercially available undoped $TiO_2$ nanoparticle under the LED lights irradiation. Fig. 10b shows the kinetic equation for N-doped $TiO_2$ naoparticle and undoped $TiO_2$ nanoparticle. The ln (Co/C) and the value of the time T are in accordance with the first-order kinetic equation y = Kx fitting. From the figure, we can see that the N-doped $TiO_2$ nanoparticle and commercially available undoped $TiO_2$ nanoparticle follows the first-order kinetic equation. The first-order kinetic equation of N-doped $TiO_2$ nanoparticle is y = 0.20579x, $R^2$ = 0.97454, and the reaction rate constant

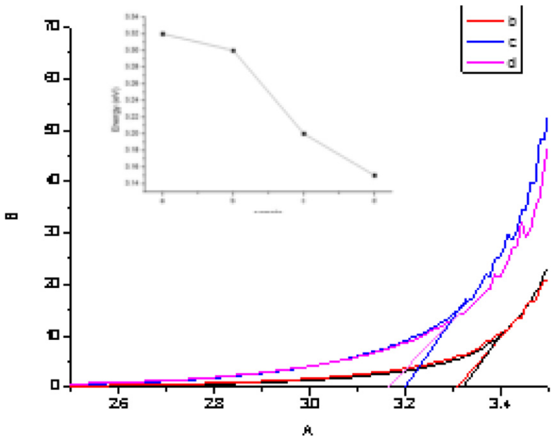


**Fig. 7** The energy gap of N-doped $TiO_2$ nanoparticle prepared in different concentrations of $NH_4Cl$. (a) Undoped $TiO_2$ nanoparticle, (b) N-doped $TiO_2$ nanoparticle prepared with 0.6 g/L $NH_4Cl$ EtOH solution, (c) N-doped $TiO_2$ nanoparticle prepared with 3.0 g/L $NH_4Cl$ EtOH solution, and (d) N-doped $TiO_2$ nanoparticle prepared with 6.0 g/L $NH_4Cl$ EtOH solution. The illustration shows the tendency of the energy gap between different N-doped $TiO_2$s.

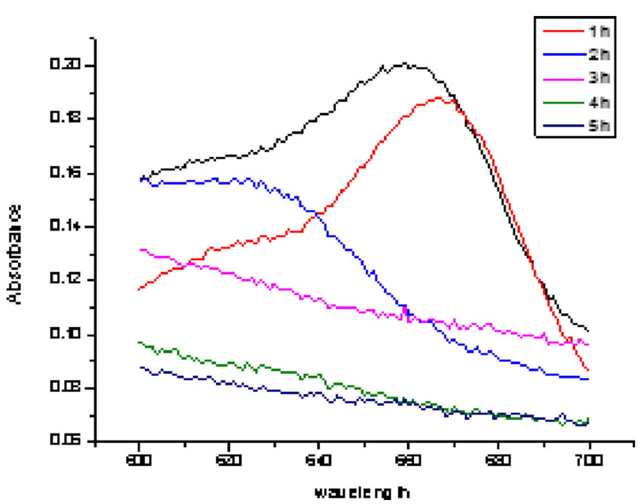


**Fig. 8** UV spectrum of N-doped $TiO_2$ nanoparticle degrading methylene blue under LED light.

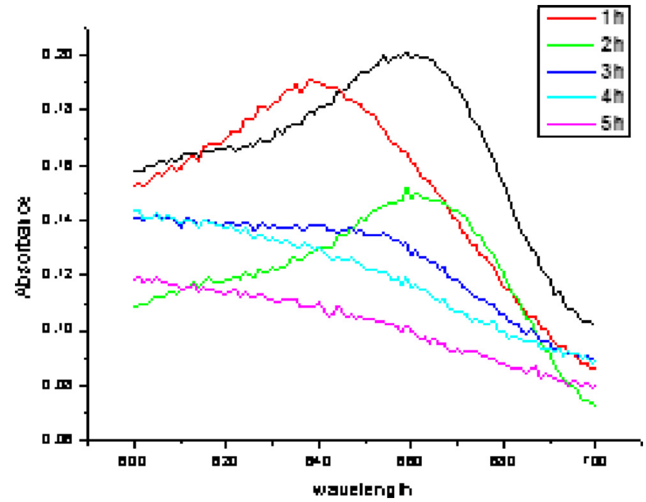


**Fig. 9** UV spectrum of commercially available undoped $TiO_2$ nanoparticle degrading methylene blue under LED light.

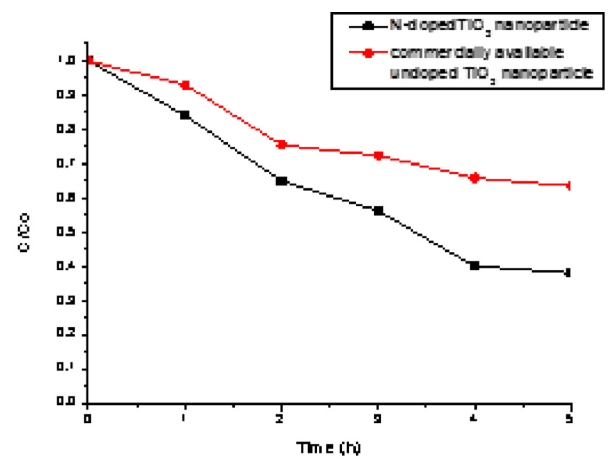


a

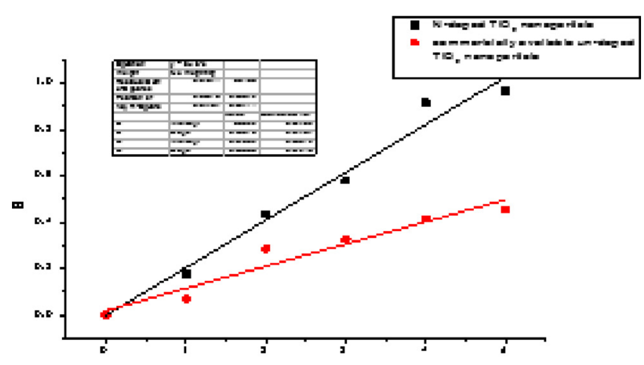

b

**Fig. 10** (a) Comparison with degradation of N-doped $TiO_2$ nanoparticle and commercially available undoped $TiO_2$ nanoparticle and (b) degradation kinetic equation.

$K_p = 0.20579$. The first-order kinetic equation of commercially available undoped $TiO_2$ nanoparticle is $y = 0.09583x$, $R^2 = 0.92471$, and the reaction rate constant $K_c$ is 0.09583. Comparing $K_p$ and $K_c$, it is clear that the reaction of N-doped $TiO_2$ nanoparticle requires less time than that of commercially available undoped $TiO_2$ nanoparticle. Fig. 11 just shows the digital image of methylene blue solution after being degraded by undoped and N-doped $TiO_2$ nanoparticle under LED light with 5 h, respectively.

Based on the results, a explanation mechanism has been proposed. In the preparation of N-doped $TiO_2$ nanoparticle, since the hydrothermal reaction, $NH_4Cl$ can be broken down into $NH_3$ and HCl during the reaction 1. And $TiO_2$ will react with $NH_3$ following the reaction Eq. (2). The fact that low-level XPS N doping was observed indicates that $NH_4Cl$ decomposition is very important for the N doping.

$$NH_4Cl \rightarrow NH_3 + HCl \quad (1)$$

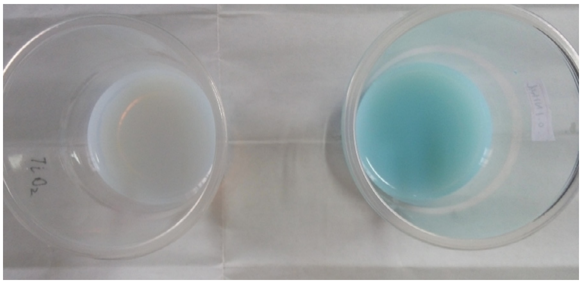


**Fig. 11** Digital image of degradating methylene blue under LED light for 5 h. N-doped $TiO_2$ nanoparticle (on the left) and commercially available undoped $TiO_2$ nanoparticle (on the right).

$$TiO_2 + NH_3 \rightarrow TiO_{2-x}N_x + H_2O \quad (2)$$

$$TiCl_4 + nH_2O \rightarrow Ti(OH)_nCl_{4-n} + nHCl \quad (3)$$

The water generated in reaction 2 will promote hydrolysis of $TiCl_4$. This is also true for reaction 3. The $Ti(OH)_nCl_{4-n}$ generated in reaction 3 will condensate further and produce $TiO_2$. The produced $TiO_2$ turns to react with $NH_3$ as reaction 2 shows. This cycle will generate the N-doped $TiO_2$ nanoparticle, according to Fig. 12.

Since $TiO_2$ is a wide band gap semiconductor, to generate electron-hole pairs under the visible light irradiation the electron in valence band cannot jump directly to the conduction band. To solve this problem, impurity level must be introduced into the band gap of $TiO_2$ by doping N atom. The reaction mechanism is shown in Fig. 13. In N-doped $TiO_2$ nanoparticle, the doped N atoms form impurity level, which is located above the valence band, so it helps reduce the energy band gap of $TiO_2$. When visible light irradiates to the N-doped $TiO_2$ nanoparticle, the electrons are excited from N2p states to transmit to the conduction band of $TiO_2$ (N2p to Ti3d) with holes left in N2p state. Based on quantum effects, the electron and hole generated by light irradiation move quickly to the surface of $TiO_2$. The only exception is that they are recombined or trapped. The excited electrons at the conduction band can transfer to new $Ti^{3+}$ states and then to deeper states of lower potential below conduction band. $Ti^{3+}$ and surface trapped electrons contribute to the photocatalytic of N-doped $TiO_2$ nanoparticle. Simultaneously, some of the generated photoelectrons will be recombined with the hole located at the N2p state (Kumar et al., 2012; Katoh et al., 2010; Berger et al., 2005). However, as the conduction band position of $TiO_2$ is $-0.5$ V vs NHE, more negative than the reduction potential ($-0.33$ V vs NHE) of $O_2/{}^{\bullet}O_2^-$, the electrons on the conduction band will react with the surface chemisorbed $O_2$ to yield the superoxide anion radicals (${}^{\bullet}O_2^-$) and further produce hydroxyl radicals (${}^{\bullet}OH$) through multi-electron reactions. Meanwhile, carbon on the surface of $TiO_2$ may serve as photosensitizer, which can be excited under visible light irradiation. These excited electrons are injected into the $TiO_2$ conduction band to play the role of sensitization (Ai et al., 2014; Chen et al., 2012). These excited electrons will react with $O_2$ absorbed on the surface of $TiO_2$ to produce ${}^{\bullet}O_2^-$ and ${}^{\bullet}OH$ subsequently. This process can increase the number of hydroxyl radicals, thereby improving the efficiency of photocatalytic. Thus, by doping N aotm into $TiO_2$ to reduce the band gap, the yield of free electron in conduction band under visible light

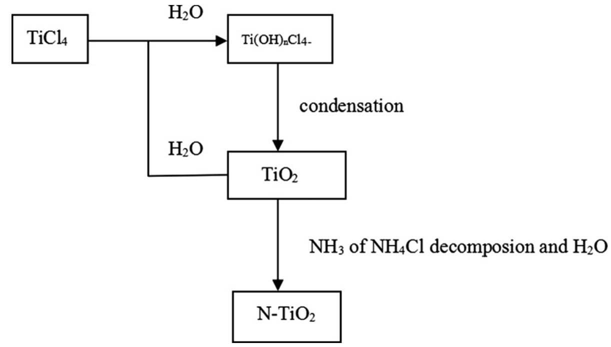


**Fig. 12** Preparing flowchart of N-doped $TiO_2$ nanoparticle.

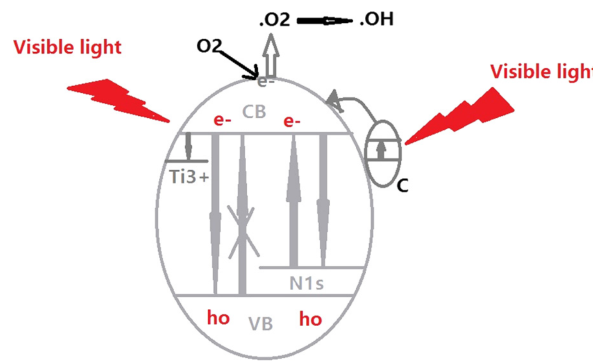


**Fig. 13** Photocatalytic mechanism of N-doped $TiO_2$ nanoparticle.

can be increased. Meanwhile, through sensitization of C atom, the number of free electrons in the conduction band can be increased to enhance the efficiency of photocatalytic. The two methods coordinate to improve the efficiency of photocatalytic for $TiO_2$ under visible light.

## 4. Conclusions

In this paper, N-doped $TiO_2$ nanoparticle was prepared by non-aqueous solvent-thermal method under low temperature. The obtained $TiO_2$ not only has high photocatalytic activity in visible light, but also shows high dispersibility in water. According to TEM and XRD characterizations, the obtained N-doped $TiO_2$ is spindle-shaped particles with the size of 8–15 nm. Based on XRD and XPS spectra analysis, it can be revealed that after N elements are doped into the $TiO_2$ lattice, the impurity level can be formed in the band gap of $TiO_2$. In this way, $TiO_2$ can extend to absorb lights from UV to visible light. The photocatalytic degradation of methylene blue experiment confirms that the photocatalytic activity of $TiO_2$ is enhanced obviously under visible light after doping with N atom. At the same time, ethanol is used as a solvent to form carbonaceous species on the surface of $TiO_2$. Then, the carbonaceous species can excite electrons into the conduction band of $TiO_2$ under visible light and increase the number of electrons in the conduction band. In this way, the visible light catalytic activity of $TiO_2$ can be increased. It is through the N doping and sensitized C that the surface state of $TiO_2$ can be changed, thereby increasing its visible light activity and high water-dispersiblity.

**Acknowledgments**

This work is financially supported by the fund of the Key Laboratory for Processing of Sugar Resources of Guangxi Higher Education Institutes (2015TZYKF02), the Scientific Research and Technology Development Project of Guangxi Province (1348018-3), and the National Natural Science Foundation of Guangxi Province (2014GXNSFAA118402).

**References**

Ai, Z.H., Wu, N., Zhang, L.Z., 2014. A nonaqueous sol–gel route to highly water dispersible $TiO_2$ nanocrystals with superior photocatalytic. Catal. Today 224, 180–187.

Asahi, R., Morikawa, T., Irie, H., Ohwaki, T., 2014. Nitrogen-doped titanium dioxide as visible-light-sensitive photocatalyst: designs, developments, and prospects. Chem. Rev. 114, 9824–9852.

Asahi, R., Morikawa, T., Ohwaki, T., Aoki, K., Taga, Y., 2001. Visible-light photocatalysis in nitrogen-doped titanium oxides. Science 392, 269–271.

Aziz, N.I.H.A., Hanafiah, M.M., 2017. The potential of Palm Oil Mill Effluent (POME) as a renewable energy source. Acta Scientifica Malay. 1 (2), 09–11.

Basheer, A.O., Hanafiah, M.M., Abdulhasan, M.J., 2017. A study on water quality from langat river. Selangor. Acta Scientifica Malay. 1 (2), 01–04.

Berger, T., Sterrer, M., Diwald, O., Panayotov, E.K.D., Thompson, T. L., Yates, J.T., 2005. Light-induced charge separation in anatase $TiO_2$ particles. J. Phys. Chem. B 109, 6061–6068.

Chen, D.M., Jiang, Z.Y., Geng, J.Q., Wang, Q., Yang, D., 2007. Carbon and nitrogen co-doped $TiO_2$ with enhanced visible-light photocatalytic activity. Eng. Chem. Res. 46, 2741–2746.

Chen, L., Chen, F., Shi, Y., Zhang, J., 2012. Preparation and visible light photocatalytic activity of a graphite-like carbonaceous surface modified $TiO_2$ photocatalyst. J. Phys. Chem. C 116, 8579–8586.

Cong, Y., Xiao, L., Zhang, J., 2006. Preparation and characterization of nitrogen-doped $TiO_2$ photocatalyst in different acid environments. Res. Chem. Intermed. 32, 717–724.

Dette, C., Pérez-Osorio, M.A., Kley, C.S., Punke, P., Patrick, C.E., Jacobson, P., Giustino, F., Soon, J.J., Kern, Klaus, 2014. $TiO_2$ anatase with a bandgap in the visible region. Nano Lett. 14 (11), 6533–6538.

Du, J., Zhao, G., Shi, Y., Yang, H., Li, Y., Zhu, G., Mao, Y., Sa, R., Wang, W., 2013. A facile method for synthesis of N-doped $TiO_2$ nanooctahedra, nanoparticles, and nanospheres and enhanced photocatalytic activity. Appl. Surf. Sci. 273, 278–286.

Elaine, M., Neville, Michael, Mattle, J., Loughrey, David, Rajesh, Bashyam, Mahfujur Rahman, J.M., MacElroy, Don, Sullivan, James A., 2012. Carbon-doped $TiO_2$ and carbon, tungsten-codoped $TiO_2$ through sol–gel processes in the presence of melamine borate: reflections through photocatalysis. J. Phys. Chem. C 116, 16511–16521.

Ghafar, F., Nazrin, T.N.N.T., Salleh, M.R.M., Hadi, N.N., Ahmad, N., Hamzah, A.A., Yusof, Z.A.M., Azman, I.N., 2017. Total phenolic content and total flavonoid content in moringa oleifera seed. Sci. Heritage J. 1 (1), 23–25.

Halim, H., Abdullah, R., Nor, M.J.M., Aziz, H.A., Rahman, N.A., 2017. Comparison between measured traffic noise in Klang Valley, Malaysia and existing prediction models. Eng. Heritage J. 1 (2), 10–14.

Halim, N.I.A., Phang, I.C., 2017. Salicylic acid mitigates pb stress in Nicotiana tabacum. Sci. Heritage J. 1 (1), 16–19.

Han, C., Liu, Y., Ma, J., He, H., 2012. Key role of organic carbon in the sunlight-enhanced atmospheric aging of soot by $O_2$. Proc. Nat. Acad. Sci. 109, 21250–21255.

Hassan, S.R., Zaman, N.Q., Dahlan, I., 2017. Influence of seed loads on start up of Modified Anaerobic Hybrid Baffled (MAHB) reactor treating recycled paper wastewater. Eng. Heritage J. 1 (2), 05–09.

Huang, Y., Ho, W., Lee, S., Zhang, L., Li, G., Yu, J.C., 2008. Effect of carbon doping on the mesoporous structure of nanocrystalline titanium dioxide and its solar-light-driven photocatalytic degradation of Nox. Langmuir 24 (7), 3510–3516.

Irie, H., Watanaba, Y., Hashimoto, K., 2003. Nitrogen-concentration dependence on photocatalytic activity of $TiO_{2-x}N_x$ powders. J. Phys. Chem. B 107, 5483–5486.

Ismail, H., Hanafiah, M.M., 2017. Management of end-of-life electrical and electronic products: the challenges and the potential solutions for management enhancement in developing countries context. Acta Scientifica Malaysia 1 (2), 05–08.

Jobbagy, M., Couselo, N., Einschlag, F.S.G., Candal, R.J., 2008. Tungsten-doped $TiO_2$ vs pure $TiO_2$ photocatalysts: effects on photobleaching kinetics and mechanism. J. Phys. Chem. C 112, 1094–1100.

Katoh, R., Furube, A., Yamanaka, K.-I., Morikawa, T., 2010. Charge separation and trapping in N-doped $TiO_2$ photocatalysts: a time-resolved microwave conductivity study. J. Phys. Chem. Lett. 1, 3261–3265.

Khan, I.U., Sajid, S., Javed, A., Sajid, S., Shah, S.U., Khan, S.N., Ullah, K., 2017. Comparative Diagnosis Of Typhoid Fever By Polymerase Chain Reaction And Widal Test In Southern Districts (Bannu, Lakki Marwat And D.I. Khan) Of Khyber Pakhtunkhwa, Pakistan. Acta Scientifica Malaysia, 1(2), 12–15.

Kiraz, N., Burunkaya, E., Kesmez, O., Camurlu, H., Asilturk, M., Yesil, Z., Ertugrul, A., 2011. Preparation of Sn doped nanometric $TiO_2$ powders by reflux and hydrothermal syntheses and their characterization. J. Sol-Gel Sci. Technol. 59, 381–386.

Kumar, A., Patel, A.S., Mohanty, T., 2012. Correlation of photodegradation efficiency with surface potential of silver-$TiO_2$ nanocomposite thin films. J. Phys. Chem. C 116, 20404–20408.

Kumar, N., Maitra, U., Hegde, V.I., Waghmare, U.V., Sundaresan, A., Rao, C.N., 2013. Synthesis, characterization, photocatalysis, and varied properties of $TiO_2$ cosubstituted with nitrogen and fluorine. Inorg. Chem. 52 (18), 10512–10519.

Li, D., Haneda, H., Shunichi Hishita, A., Ohashi, N., 2005. Visible-light-driven N-F-codoped $TiO_2$ photocatalysts. 1. Synthesis by spray pyrolysis and surface characterization. Chem. Mater. 17, 2588–2595.

Periyat, P., McCormack, D.E., Hinder, S.J., Pillai, S.C., 2009. One-pot synthesis of anionic (nitrogen) and cationic (sulfur) codoped high-temperature stable, visible light active, anatase photocatalysts. J. Phys. Chem. C 113, 3246–3253.

Rahman, N.A., Halim, H., Gotoh, H., Harada, E., 2017. Validation of microscopic dynamics of grouping pedestrians behavior: from observation to modeling and simulation. Eng. Heritage J. 1 (2), 15–18.

Razali, M.A.A., Said, F.M., 2017. Red pigment production by monascus purpureus in stirred-drum bioreactor. Sci. Heritage J. 1 (1), 13–15.

Sakthivel, S., Janczarek, M., Kisch, H., 2004. Visible light activity and photoelectrochemical properties of nitrogen-doped $TiO_2$. J. Phys. Chem. B 108, 19384–19387.

Serpone, N., 2006. Is the band gap of pristine $TiO_2$ narrowed by anion- and cation-doping of titanium dioxide in second-generation photocatalysts. J. Phys. Chem. B 110, 24287–24293.

Shamsudin, N.H., Wong, C.H., Rahman, R.N.Z.R.A., Ali, M.S.M., 2017. Tight repression of elastase strain K overexpression by Pt7 (A1/O4/O3) shuttle expression system. Sci. Heritage J. 1 (1), 20–22.

Shan, G.B., Demopoulos, G.P., 2010. The synthesis of aqueous-dispersible anatase $TiO_2$ nanoplatelets. Nanotechnology 21, 025604–025609.

Sukor, N.S.A., Jarani, N., Fisal, S.F.M., 2017. Analysis of passengers' access and egress characteristics to the train station. Eng. Heritage J. 1 (2), 01–04.

Sun, L., Zhao, Z.L., Zhou, Y.C., Liu, L., 2012. Anatase $TiO_2$ nanocrystals with exposed 001 facets on graphene sheets via molecular grafting for enhanced photocatalytic activity. Nanoscale 4, 613.

Tachikawa, T., Tojo, S., Kawai, K., Endo, M., Fujitsuka, M., Ohno, T., Nishijima, K., Miyamoto, Z., Majima, T., 2004. Influence of metal ions on the charge recombination processes during $TiO_2$ photocatalytic one-electron oxidation reactions. J. Phys. Chem. B 108, 19299–19306.

Tahir, M.N., Theato, P., Oberle, P., Melnyk, G., Faiss, S., Kolb, U., Janshoff, A., Stepputat, M., Tremel, W., 2006. Facile synthesis and characterization of functionalized, monocrystalline rutile $TiO_2$ nanorods. Langmuir 22, 5209–5212.

Tian, L., Deng, K., Ye, L., Zan, L., 2011. Effect of surface ethoxy groups on photoactivity of $TiO_2$ nanocrystals. Appl. Surf. Sci. 257, 10653–10658.

Yu, A.M., Wu, G.J., Zhang, F.X., Yang, Y.L., Guan, N.J., 2009. Synthesis and characterization of N-doped $TiO_2$ nanowires with visible light response. Catal. Lett. 129, 507–512.

Yurdakal, S., Palmisano, G., Loddo, V., Augugliaro, V., Palmisano, L., 2008. Nanostructured rutile $TiO_2$ for selective photocatalytic oxidation of aromatic alcohols to aldehydes in water. J. Am. Chem. Soc. 130 (5), 1568–1569.

Zhang, X.F., Zhang, B.Y., Zuo, Z.X., Wang, M.K., Shen, Y., 2015. N/Si co-doped oriented single crystalline rutile $TiO_2$ nanorods for photoelectrochemical water splitting. J. Mater. Chem. A 3, 10020–10025.

Zhu, J., Zhang, D., Bian, Z., Li, G., Huo, Y., Lu, Y., Li, H., 2009. Aerosol-spraying synthesis of $SiO_2/TiO_2$ nanocomposites and conversion to porous $TiO_2$ and single-crystalline $TiOF_2$. Chem. Commun. 36, 5394.